Vol. 55 · No. 4
ISSN 0091-3286

April 2016

Optical Engineering

OpticalEngineering.SPIEDigitalLibrary.org

SPIE.

Optical Engineering

OpticalEngineering.SPIEDigitalLibrary.org

Enhanced optical discrimination system based on switchable retroreflective films

Phillip Schultz
Jason Heikenfeld

SPIE.

Phillip Schultz, Jason Heikenfeld, "Enhanced optical discrimination system based on switchable retroreflective films," *Opt. Eng.* **55**(4), 045101 (2016), doi: 10.1117/1.OE.55.4.045101.

Enhanced optical discrimination system based on switchable retroreflective films

Phillip Schultz and Jason Heikenfeld*
University of Cincinnati, Department of Electrical Engineering and Computing Systems, Novel Devices Laboratory, Cincinnati, Ohio 45221, United States

Abstract. Reported herein is the design, characterization, and demonstration of a laser interrogation and response optical discrimination system based on large-area corner-cube retroreflective films. The switchable retroreflective films use light-scattering liquid crystal to modulate retroreflected intensity. The system can operate with multiple wavelengths (visible to infrared) and includes variable divergence optics for irradiance adjustments and ease of system alignment. The electronic receiver and switchable retroreflector offer low-power operation (<4 mW standby) on coin cell batteries with rapid interrogation to retroreflected signal reception response times (<15 ms). The entire switchable retroreflector film is <1 mm thick and is flexible for optimal placement and increased angular response. The system was demonstrated in high ambient lighting conditions (daylight, 18k lux) with a visible 10-mW output 635-nm source out to a distance of 400 m (naked eye detection). Nighttime demonstrations were performed using a 1.5-mW, 850-nm infrared laser diode out to a distance of 400 m using a night vision camera. This system could have tagging and conspicuity applications in commercial or military settings. [DOI: 10.1117/1.OE.55.4.045101]

Keywords: retroreflector; optics; laser; electronics; films; electro-optics; liquid crystal; corner cube.

Paper 151822 received Dec. 24, 2015; accepted for publication Mar. 1, 2016; published online Mar. 28, 2016.

1 Introduction

Range-finding[1] and general conspicuity[2] have long exploited the efficient and predictable optical properties of retroreflectors. By reflecting incident light back to the source in a narrow beam, retroreflectors offer substantially higher contrast compared to diffusely reflecting surroundings. Adding a means to switch on or off the retroreflected light provides additional advantages, including (1) increased conspicuity,[3] (2) ability to allow or disallow retroreflection as needed, and (3) the potential for free-space optical communications. Free-space optical communications has been the field most heavily investigated for switchable retroreflectors. Prior approaches include microelectromechanical systems (MEMS)[4] and multiple quantum wells (MQW).[5–7] Though these previous approaches do exhibit high switching speeds,[8] they suffer from narrow spectral band operation, low contrast, small retroreflective area, and challenging optical system alignment. These challenges are particularly undesirable for applications in naked eye conspicuity. Our group had previously reported an electrowetting light scattering switchable retroreflector[9–12] to overcome these challenges, which we recently improved upon through a liquid crystal modulator.[13] Our new approach does not provide the high switching speeds of the previous MEMS and MQW methods, but provides superior performance in nearly all other metrics of interest to conspicuity applications: high contrast of >2000:1 at 635 nm and >400:1 at 850 nm, large area of 75 cm^2, visible and infrared spectrum from 400 to 1600 nm, and thin-flexible construction at <0.6 mm thickness.

We report here a system-level demonstration, which is the culmination of our continuum of effort to create an enhanced optical discrimination system based on switchable retroreflective films. In this paper, physics, design, and characterization of the retroreflective film are first discussed, followed by a description of the electronic interrogation and response system. An optical model is provided showing theoretical long-distance viewing of the films with both naked eye and night vision (NVIS) viewing for day and nighttime conditions. The model is then verified with various field demonstrations, confirming the ability to integrate such a system into conspicuity applications.

2 System Description

A laser interrogation and response system was integrated with the switchable retroreflective films to provide a way to remotely actuate the films from a distance by means of a single operator.

2.1 *Introduction*

The basic operational goals for the system were to provide a means of interrogating and actuating the switchable retroreflective films with only specific light sources, and to limit access to the reflected signal. The block diagram in Fig. 1 shows the general system solution utilized to achieve these goals. Referring to Fig. 1, the system can be realized with two main blocks: an interrogator and a receiver.

The interrogator is enabled by the user by depressing a push button. The interrogator has two basic functions: (1) provide a light source that can be seen by an individual by naked eye or NVIS after retroreflection and (2) provide an encoded signal to the receiver to tell it to actuate (retroreflect). These were achieved by the use of laser diodes with an encoded data/pulse stream.

*Address all correspondence to: Jason Heikenfeld, E-mail: heikenjc@ucmail.uc.edu

0091-3286/2016/$25.00 © 2016 SPIE

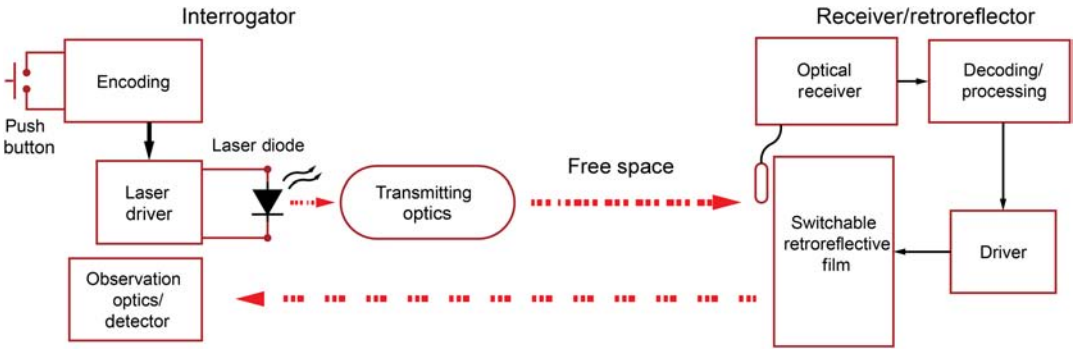

Fig. 1 Block diagram of the interrogator and receiver/retroreflector.

The receiver block functions include (1) receiving the interrogating optical signal (wavelength and code), (2) decoding the signal and processing it to determine if it matches the stored code, and (3) driving the switchable retroreflective film if matching is successful. When the retroreflective film is electrically powered, the interrogating light will be retroreflected back to the viewer through the interrogator's observation optics.

In order to choose the appropriate parameters for the full system, the retroreflective films first needed to be fully characterized and modeled. This then allows predictive system-level design, especially when attempting long-distance operation.

2.2 *Retroreflector Film Characterization*

The primary optical component of the switchable retroreflective film is a microreplicated array of corner-cube retroreflectors.[14,15] As shown in Fig. 2, each corner cube is composed of three orthogonally connected mirrors forming an inverted trihedral reflector. Incident light enters the aperture and reflects off all three surfaces, the last of which reflects the light back in the direction of, but parallel to, the incident light in a narrow cone of $\sim \pm 0.2$ deg. Figure 2(c) shows the normalized retroreflected intensity response due to incident angle for the bare retroreflective film. A line fit was provided by the following heuristic model:[16]

$$R(\theta) = R_{\mathrm{MAX}} \cos \theta^{\gamma}, \tag{1}$$

where R_{MAX} is the maximum retroreflected intensity in units of retroreflected percent (at $\theta = 0$) and γ is the heuristic parameter for best line fit. For the films used herein, it was determined that $\gamma = 5.25$ agrees well with all wavelengths measured ($\lambda = 400$ to 1000 nm).

As shown in Fig. 3, the electro-optical switching is performed by adding a polymer dispersed liquid crystal (PDLC) shutter,[17–19] whose fabrication is discussed elsewhere.[20–22] The PDLC films used for this study were purchased through Polytronix Inc. of Richardson, Texas.

PDLC consists of several randomly oriented droplets of liquid crystal (location and angle) in a suspending polymer. In the off state, incident light scatters due to the mismatch of refractive indices between the birefringent liquid crystal and the suspending polymer, causing a diffuse reflection (no retroreflection). When voltage is applied, the liquid crystal droplets align with the electric field. In this uniform orientation, the liquid crystal and suspending polymer have nearly

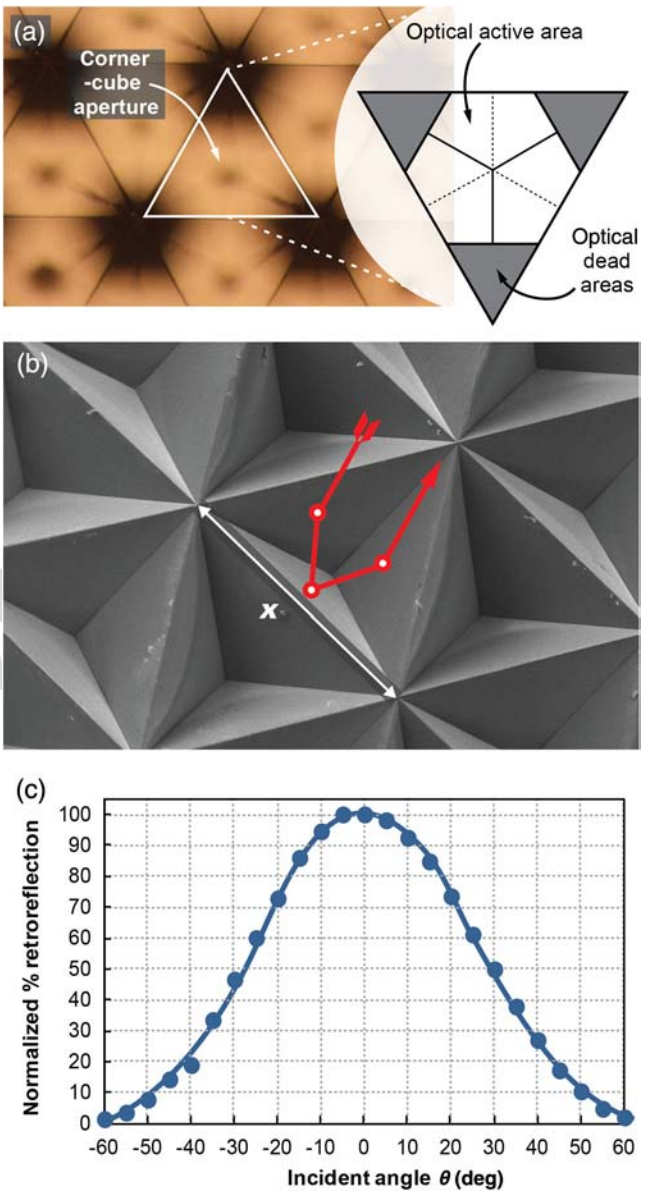

Fig. 2 Fundamentals of corner-cube retroreflectors: (a) collinear top view of a corner-cube array with on-axis incident light showing the active and dead areas of a single cube. (b) SEM of a corner cube with an example ray trace. Corner cube side wall lengths, x, are typically on the order of 150 to 800 microns for sheeting materials, and 175 microns for the films used herein. (c) Retroreflection intensity versus input angle of the retroreflective film measured using the characterization setup of Fig. 6(b) for 635 nm with the points being measured data and the line being a heuristic fit curve from Eq. (1).

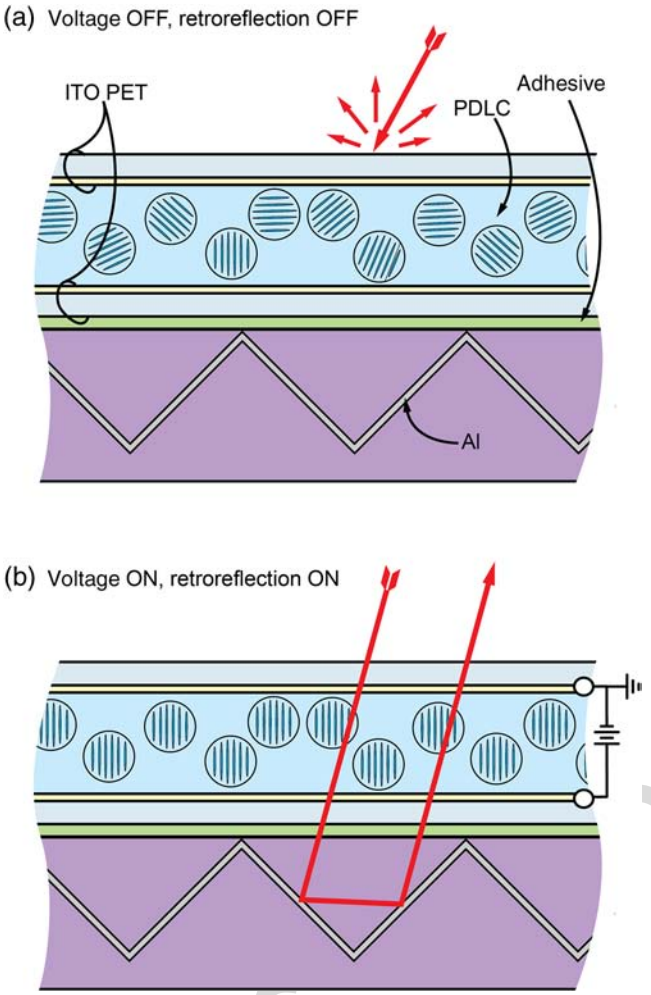

Fig. 3 Polymer-dispersed liquid crystal switchable retroreflective film in its (a) voltage OFF/scattering state and (b) voltage ON/retroreflecting state. This is not drawn to scale and for illustration purposes only. Droplet diameters are normally on the scale of <10 microns, while the corner cube side wall lengths (x from Fig. 2) are on the order of >100 microns.

matched refractive indices, making the films optically clear, allowing retroreflection. Different materials and processing chosen can allow tuning of the film with respect to angular response, spectral response, applied voltage, and switching speeds. The films used herein were not optimized for this work.

The inorganic layers in the device are very thin, specifically ~100 nm $In_2O_3:SnO_2$ electrodes (indium tin oxide) and ~100 nm of reflective Al. All other materials are polymers, and therefore, the entire device can be bent to a radius of curvature of <5 cm. Images of the films in operation can be seen in Fig. 4 with the on state showing high retroreflected intensity when observation is performed in line with the interrogating light, and attenuation of the retroreflected light when observed slightly off axis beyond 0.2 deg.

The setup shown in Fig. 5 was used to characterize the on/off retroreflection response versus wavelength and angle for the switchable retroreflective films. It consists of a 150 W MR16 halogen lamp (Osram 54732) coupled into an optical fiber (Ocean Optics P200-2-VIS-NIR). The output was collimated with a 200 mm biconvex lens placed 200 mm from the end of the fiber. The aperture was placed just before the

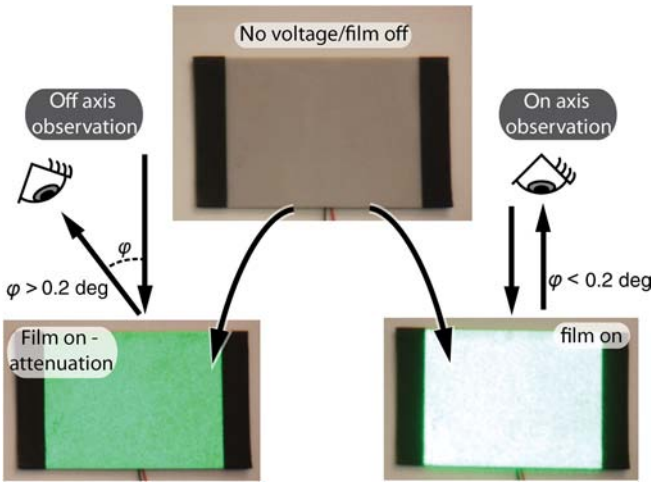

Fig. 4 Images showing the operation of the PDLC switchable retroreflector in its voltage off/scattering state, voltage on/retroreflecting state with viewing slightly off axis to show the color and attenuation, and retroreflecting with viewing on axis with the light source.

lens and adjusted to provide the desired diameter spot. Collimated light was then split by a nonpolarizing beam splitter and adjusted to be incident on the switchable retroreflector. Retroreflection could then reflect light to transmit back through the beam splitter and be incident on the collimator attached to a fiber optic cable (Ocean Optics QP600-1-SR) located ~31 cm from the retroreflector to collect retroreflected light within a ±0.2 deg cone. The collected light was then guided into a spectrometer (Ocean Optics HR4000-CG-UV-NIR) in which data were analyzed using Ocean Optics SpectraSuite version 1.4.2. As a reference, a bare retroreflector film was used and angled slightly by ~2 deg to eliminate specular reflection. The collimator and 0.6-mm fiber were then adjusted to provide the maximum retroreflected reading.

The results of the setup from Fig. 5 are plotted in Fig. 6. As shown in Fig. 6(a), comparing the on/off retroreflection response as a function of incident angle yields a maximum reflection that is 57% of the response of the bare reference retroreflective film. The spectral response was also measured [Fig. 6(b)] at 0 deg incident angle and shows high contrast

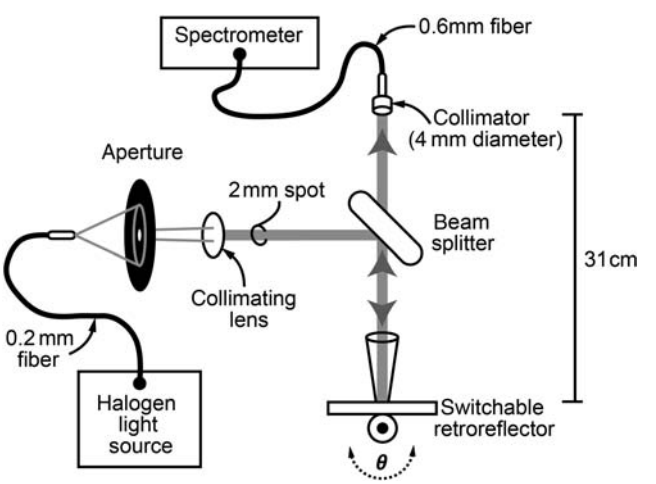

Fig. 5 Setup used to characterize the spectral response of the switchable retroreflective film.

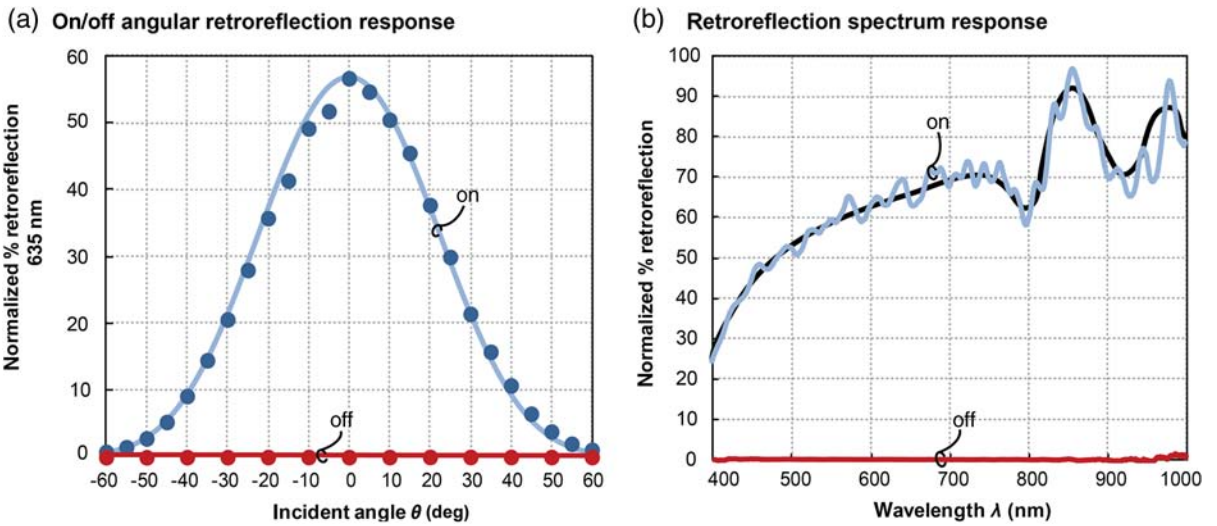

Fig. 6 (a) Retroreflection intensity versus input angle for the PDLC retroreflective film in its on and off states with data collected for 635 nm with the characterization setup shown in Fig. 5. Points are measured and the "on" line is the heuristic fit curve using Eq. (1) with $\gamma = 6.85$. (b) On/off percent of retroreflection versus wavelength from 400 to 1000 nm, calibrated to a bare retroreflector film. The blue line is the measured data with the black overlay being a trend curve.

over a broad spectrum from 400 to 1000 nm (encompassing visual and infrared/NVIS wavelengths). The nonuniformity of the collected data is suspected to be due to several thin film interference effects.

Also measured with the setup from Fig. 5 was the angular wavelength response due to incident angle. The inverse proportionality of the retroreflection percentage due to the increase in incident angle remained similar throughout the spectrum. The main difference was apparent at angles beyond the standard field of view, in which a select few can be seen in Fig. 7. For the bare retroreflective film, these incident angles were between 71 and 77 deg with relatively consistent intensities between ~11 and 13% of the max retroreflection for any given wavelength. The switchable films showed a substantial decrease and shift of the diffraction spectral envelope with angles between 57 and 59 deg. The intensity was not consistent however with the near-infrared wavelengths (~715 to 900 nm) showing a higher intensity (approximate slope linearity from 13 to 22%, respectively). The visible wavelength intensities, however, were lower from ~3 to 13% (approximate linear slope) of the max bare film retroreflection for 400 to 715 nm.

We discussed this phenomenon with retroreflective film optical designers. The leading speculation was that it is due to the reflections from two of the facets of a given corner cube at a high incident angle. Any light being returned will be traveling through more polymer than usual, causing white light dispersion, which could influence the change in angle of return. However, we have no direct evidence to support this speculation at this time.

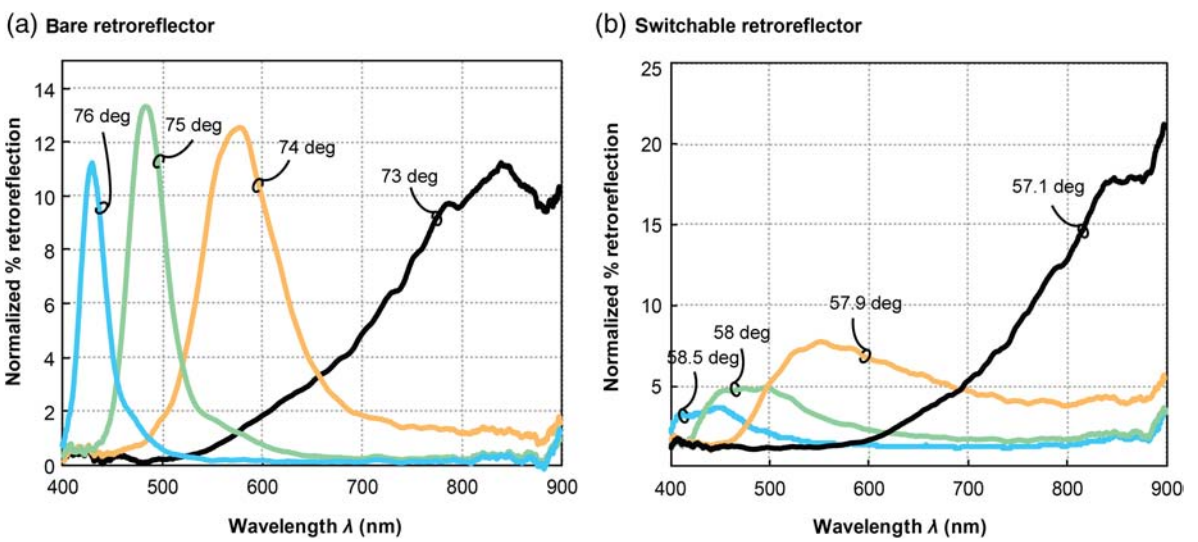

Fig. 7 Spectral responses at select input angles as a function of percent retroreflection versus wavelength as measured using the characterization setup shown in Fig. 5 for (a) a bare retroreflector film and (b) the switchable retroreflector film.

2.3 *Electronics and Optics Design and Integration*

The following electronics and optics for the interrogation and response prototype were developed and assembled with components from both NGC Xetron (Cincinnati, Ohio) and at the University of Cincinnati.

2.3.1 *Interrogator*

The interrogator had the requirement to be able to modulate a light source and provide a small packet of data and relatively uniform illumination of a target from distances of 10 m out to as much as 1 km. A block diagram and optics train of the pursued solution for the interrogator is shown in Fig. 8.

The interrogator is a microcontroller-driven laser diode with a push-button user interface. A bare laser diode output has a highly divergent elliptical shape (± 5 to 10 deg and ± 15 to 30 deg axis based) that requires beam shaping along each axis to circularize it. Shaping was implemented by the use of plano-concave cylindrical lenses oriented based on the axis they needed to shape. The higher diverging axis uses two lenses ($f = 15$ and 25.4 mm) spaced 8 and 15 mm (respectively) from the laser output to provide an ~12.7-mm-diameter collimated beam. The beam trace for this path is shown in dark red prior to the aperture in Fig. 8. The lower divergence axis uses only one $f = 40$ mm lens placed 40 mm from the source for collimation. This trace is shown in yellow prior to the aperture in Fig. 8. The beam then passes through the 12.7-mm-diameter circular aperture for final beam shaping. The output lenses ($f_4 = -25$ mm and $f_5 = 50$ mm) provide the controlled expansion/collimation for a beam of ~25.4 mm output diameter (bright red trace post aperture). Variable divergence is accomplished by adjusting f_4 from its collimating position (f_{4A}) closer to f_5 (position f_{4B}). This provides a maximum divergence of $\sim \pm 5$ deg. The output trace adjustment for this is shown with the dashed orange lines.

Power consumption is on the order of 30 mW with the laser off (standby) and 300 mW with the laser being driven. It currently runs on 2× CR123A batteries in series. Simple relocation of the push-button switch can allow for zero battery drain, which would limit the battery life to the number of interrogations at the expense of increasing the system response time.

2.3.2 *Receiver*

The basic function of the receiver was to take in the optical signal (data/code) from the interrogator, process it, confirm the code is correct, and then drive the switchable retroreflective film. The receiver also needs to function in a broad range of ambient light conditions (night and daylight) and with multiple laser source wavelengths. The receiver also should be able to operate with low enough power to be able to use small, lightweight batteries (coin cell). Figure 9 shows the block diagram of the electronic solution used for the receiver.

The front end consists of a PIN photodiode. Typical PIN photodiodes have spectral sensitivities from ~200 to 1100 nm, with their highest sensitivities (typ.) in the 850 nm range, making them ideal for this system. The received optical signal induces a current by the photodiode, which is fed into a transimpedance amplifier (TIA) to convert it to a voltage and amplify the signal. Ambient light is received and passes the TIA as direct current. This is filtered out with a high-pass filter. Higher frequencies are filtered out with a low-pass filter integrated into the feedback of the TIA, further reducing the processed bandwidth. The signal is then shifted up to modulate around a reference voltage, provided by the reference buffer, and further amplified with a voltage summing amplifier. This provides a signal large enough to recreate the received data using a comparator with the same reference voltage as used in the summing stage. The reconstituted data are input directly into a microcontroller, where it is read and compared to the stored code. If the codes match, then the microcontroller signals the switchable retroreflector's driver to modulate the incident light.

The receiver/driver current standby power consumption is <4 mW and can run on 2× CR2032 coin cell batteries for ~100 h. With further optimization, consumption can be closer to 0.3 mW and would be able to operate on one CR2032 coin cell battery (225 mAh) for >1500 h. Operation in daylight conditions does require optical filtration on the photodiode, of which the transmission spectrum shown in Fig. 10 is for the custom assembled filter used in this study. No such filter is needed for nighttime conditions. The receiver's limit on optical irradiance and the associated spot sizes for the various laser diodes used are shown in Table 1 (and will be discussed in more detail in Sec. 3).

Though not currently built in, it is possible for the receiver to return confirmatory data for an all-around free-space communication system with low data rates (Hz). It would be

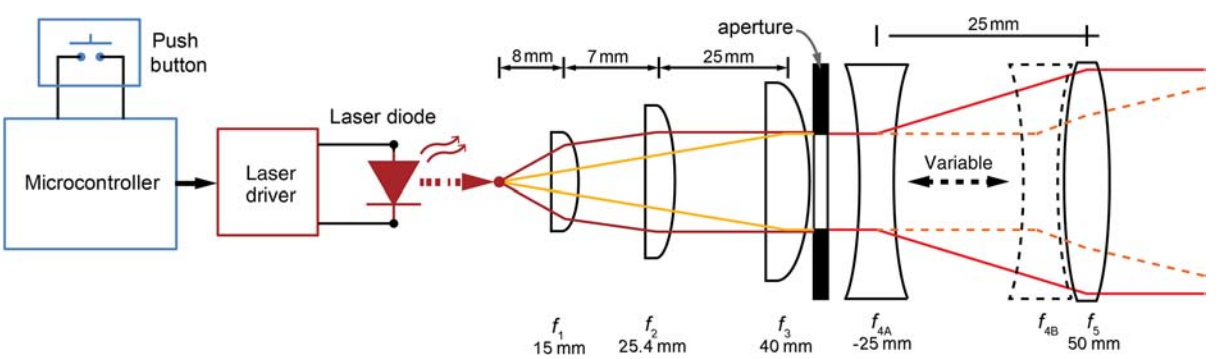

Fig. 8 Interrogator and electronics block diagram feeding into its optics train. A bare laser diode has an elliptical output, which requires beam-shaping along each axis as shown with the different ray trace colors (red versus yellow). The optics provide variable divergence as shown with the dashed secondary location of f_4 (f_{4B}) providing the subsequent dashed ray trace.

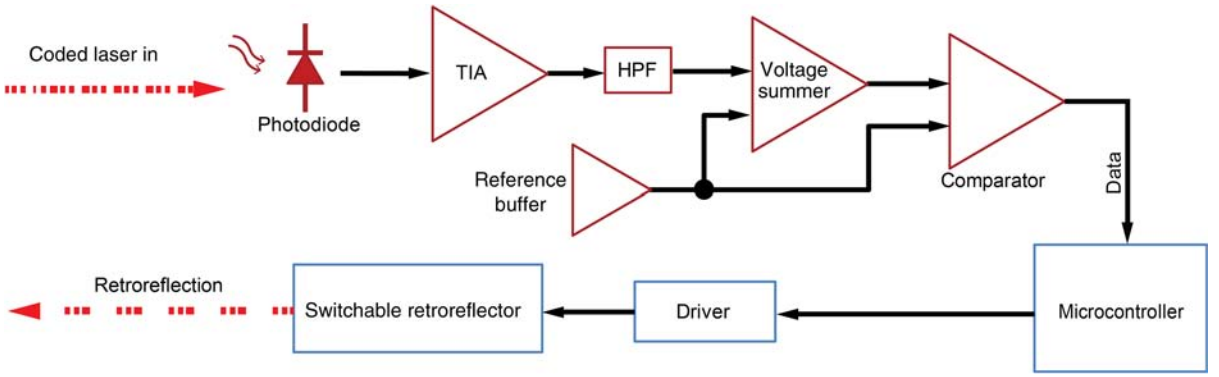

Fig. 9 Receiver/switchable retroreflector driver electronics block diagram. The optical reception and analog circuitry are shown in red, while the digital portion is shown in blue.

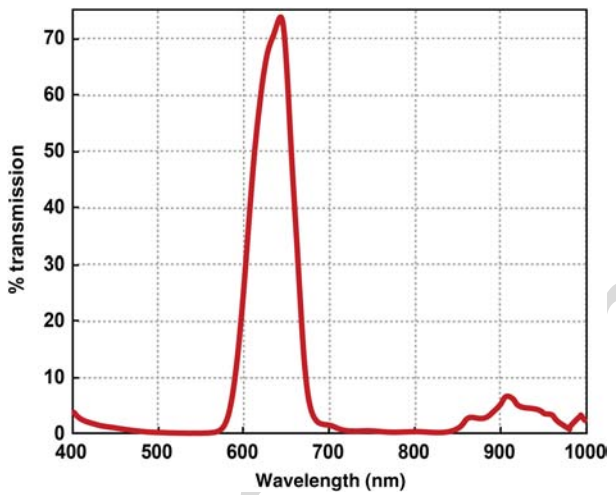

Fig. 10 Custom optical bandpass filter used for daytime demonstrations.

possible to return location data if GPS were integrated into the system, or various other user input data streams.

2.3.3 *System*

The completed system can be seen in Fig. 11. The interrogator, shown in Fig. 11(a), is set up to be able to mount to a spotting scope for simple alignment/zeroing with viewing optics, as shown in Fig. 11(c) with a spotting scope.

The setup shown in Fig. 12(a) was used to characterize the system temporal response from the initial push button press to 90% of the maximum retroreflected response. The setup uses a 0.5 mW HeNe laser (Melles Griot 05-SRP-810). The HeNe beam is split and directed to the switchable retroreflector with a beam splitter. The photodetector (Newport 918C-SL-OD3) was aligned to receive the retroreflected signal using a base retroreflective film. The analog output of the optical power meter (Newport 1918-C) is connected to an oscilloscope along with the output of the push button. The oscilloscope is set to trigger with the rising edge signal created by the depression of the push button. The fastest theoretical response of the system is 8.35 ms. The fastest achieved response was 9 ms; however, 10 to 15 ms is more typical as shown in the oscilloscope screenshot of Fig. 12(b).

3 Optical Model for Maximum Distance

Understanding the maximum distances at which the system can operate has obvious value from an applied perspective and is also interesting theoretically in terms of the optics/physics involved. From an optical perspective, the system can be viewed as two divergent radiators separated by a certain distance in free space with air in between. In this case, we can use geometric means to calculate the returned optical power when the switchable retroreflector is oriented at 0 deg. A diagram of this optical model is shown in Fig. 13, which can be described as follows.

The only relevant light coming into the system is from the interrogating light source. All other variables in the system

Table 1 Laser diode limits for receiver detectable spot sizes and associated irradiances with/without a filtered photodiode (see Fig. 10).

			Max spot diameter		Min spot diameter		Min irradiance		Max irradiance	
Wavelength (nm)	Laser power (mW)	Output power (mW)	Filtered (m)	No filter (m)	Filtered (cm)	No filter (cm)	Filtered (nW/cm^2)	No filter (nW/cm^2)	Filtered (mW/cm^2)	No filter (mW/cm^2)
635	5	2.5	1.4	1.7	1.6	1.8				
	10	4.5	1.9	2.3	2.1	2.4	153.5	104.4	1.25	1.02
	20	10	2.9	3.5	3.2	3.5				
850	5	1.5	—	1.5	—	1.5	—	87.55	—	0.85
	10	3.2	—	2.2	—	2.2				

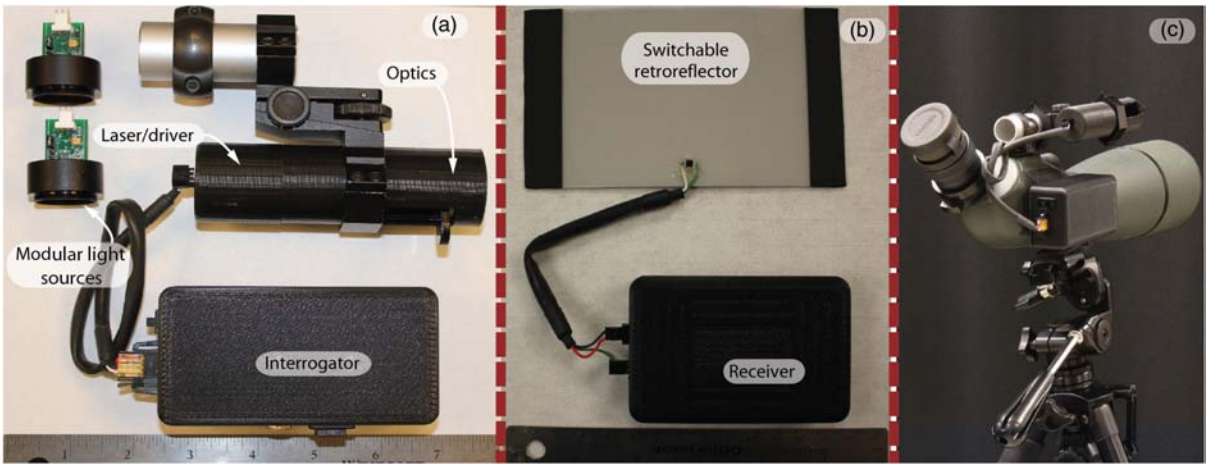

Fig. 11 Image of the (a) interrogator and optics, (b) receiver and tag, and (c) example interrogator setup with a spotting scope. The ruler shown at the bottom of (a) is in inches, and (b) is in cm.

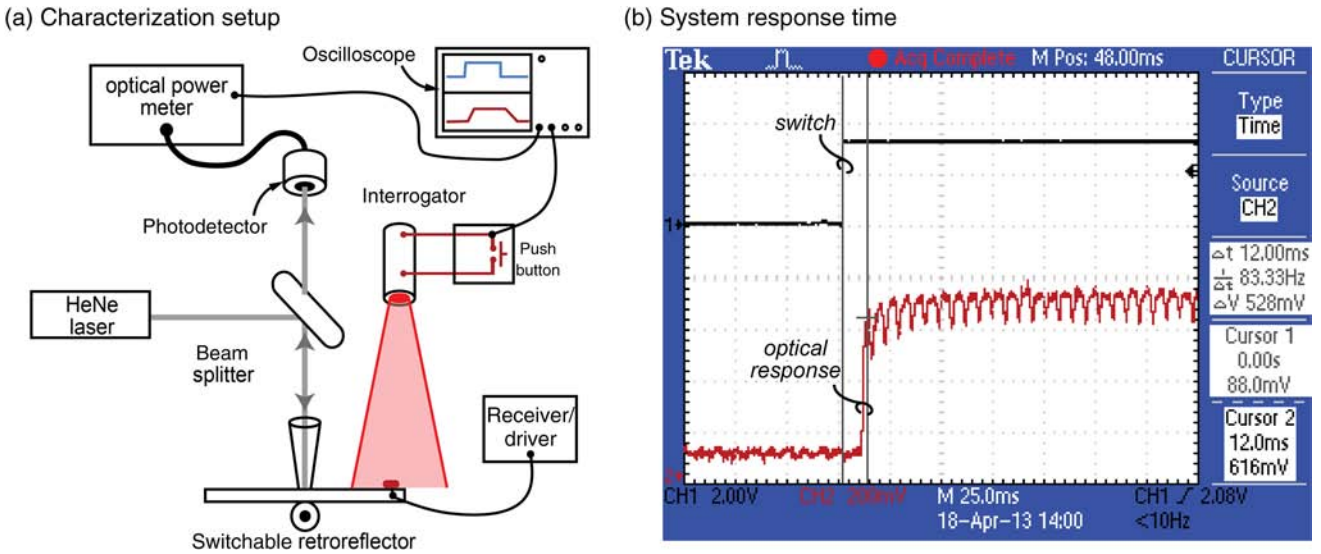

Fig. 12 (a) Characterization setup to measure the temporal response and (b) oscilloscope screenshot of the system temporal response showing both the push-button depression (top black line) and the total response time of the receiver as it turns on the retroreflector film (bottom red line).

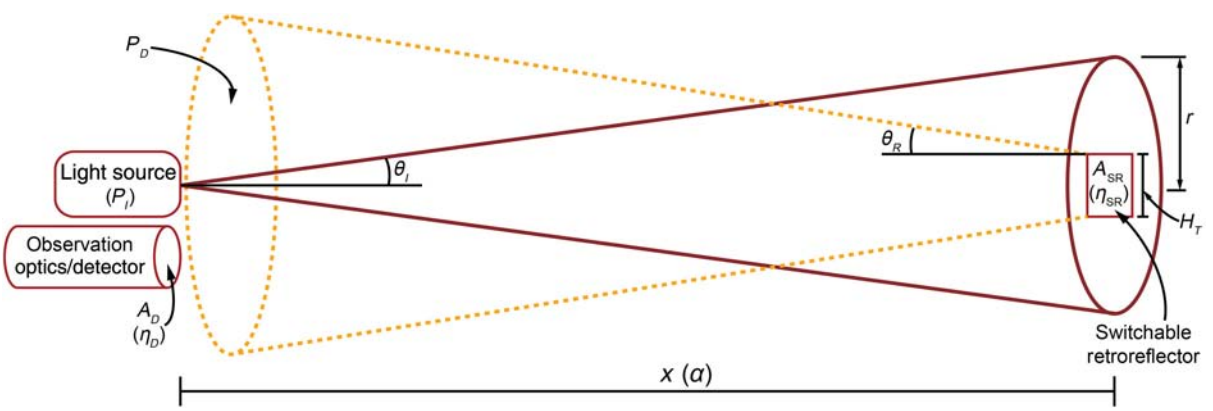

Fig. 13 Diagram of the optical model of the system.

will affect this to determine what is actually detected. Incident irradiance (E_I) on the retroreflector can be expressed as

$$E_I = \frac{P_I e^{-\alpha x(\mathrm{km})}}{\pi r^2}, \tag{2}$$

where P_I is the light source's output optical power (mW), α is the ambient attenuation coefficient (dB/km), x is the distance between the light source and film, and r is the radius of the incident spot on the retroreflector (cm).

The effect the switchable retroreflector has on the incident irradiance to provide the return beam can be expressed as

$$E_R = E_I \cdot \frac{A_{\mathrm{SR}} \eta_{\mathrm{SR}} e^{-\alpha x(\mathrm{km})}}{\pi [x(\mathrm{cm}) \tan \theta_R + H_{\mathrm{SR}}/2]^2}, \tag{3}$$

where A_{SR} is the area of the switchable retroreflector (cm^2), η_{SR} is the retroreflector efficiency coefficient, θ_R is the retroreflected divergence, and H_{SR} is the height of the film (cm). A second attenuation is introduced due to the retroreflected beam transmitting through the same free-space distance as the incident light.

The observation optics and detector have an associated optical acceptance area (A_D in cm^2) and efficiency (η_D). Combining this with Eqs. (2) and (3) provides a complete expression for the detected optical power (P_D in mW) for a given detector area.

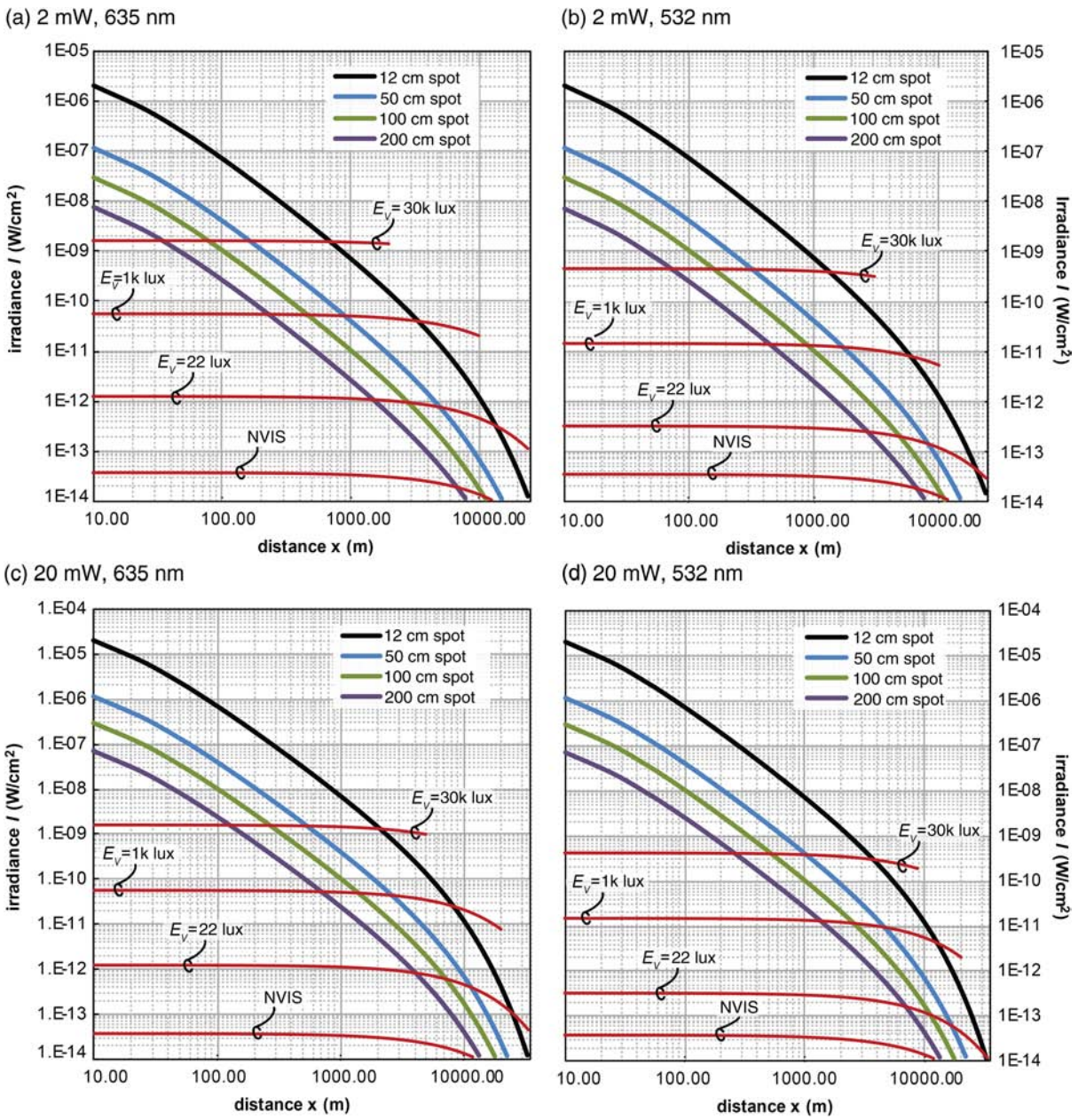

Fig. 14 Theoretical plots of retroreflected irradiance (I) as a function of distance (x) for various interrogator spot sizes (12, 50, 100, and 200 cm), laser powers [(a) and (b) 2 mW, (c) and (d) 20 mW], and laser wavelengths [(a) and (c) 635 nm, (b) and (d) 532 nm), at the tag. The horizontal red plots show human eye photopic threshold levels for various ambient illuminance (E_v) levels along with an example NVIS threshold at 850 nm.

$$P_D = \frac{P_I A_{SR} A_D e^{-2\alpha x(\mathrm{km})} \eta_{SR} \eta_D}{\pi^2 r^2 [x(\mathrm{cm}) \tan \theta_R + H_T/2]^2}. \quad (4)$$

By setting A_D to a unitless value of 1, one can calculate the detectable irradiance in units of $\mathrm{mW/cm^2}$.

Equation (4) can be alternatively expressed with the light source's divergence (θ_I) instead of incident spot radius by setting $r = x \tan \theta_I$. Equation (4) assumes that the incident light is uniform and fully illuminating the switchable retroreflector, the incident and retroreflected beams are circular, and that the light source/laser is a point source. Example curves (irradiance versus distance) can be seen in Fig. 14 for various spot diameters, laser outputs, and wavelengths on log-log plots. Angular orientation can also be taken into account by adjusting Eq. (4).

$$P_D(\theta) = P_D \cos \theta^{\gamma}, \quad (5)$$

with $\gamma = 6.85$ for these films.

The irradiance plots in Fig. 14 are only meaningful from an applications perspective if minimum detection power can be understood on the interrogator end of the system. Therefore, a model is also provided to determine the irradiance threshold levels necessary for naked eye visualization. This is based on the background surrounding the retroreflective films having an associated reflection coefficient (albedo) of sunlight. This can be modeled by assuming the surroundings are diffuse reflectors[23,24] using a form of Lambert's cosine law[25] for the received optical power on the detector due to ambient reflections (P_{DA}).

Table 2 Values used for calculations.

Description	Variable	Value	Units
Retroreflected irradiance			
Attenuation coefficient	α	0.1	dB/km
Switchable retroreflector area	A_{SR}	77.4	$\mathrm{cm^2}$
Switchable retroreflector efficiency coefficient	η_{SR}	0.25	—
Switchable retroreflector height	H_{SR}	7.62	cm
Retroreflected beam divergence angle	θ_R	0.2	deg
Observation optics and detector area	A_D	1	—
Observation optics and detector efficiency	η_D	1	—
Naked eye thresholds			
Ambient illuminance	E_V	22 to 30k	lux
Detector area	A_D	0.0001	$\mathrm{m^2}$
Observation angle	θ_O	80	deg
Field of view angle	θ_{FOV}	1	deg
Reflection coefficient	R	0.3	—
Contrast change[26]	C	0.006	—

$$P_{DA} = \frac{P_{AI} A_D \cos \theta_O}{\pi x^2}, \quad (6)$$

where P_{AI} is the incident ambient light on the surface of the background, A_D is the area of the detector aperture, θ_O is the observation angle between the ambient light source on the retroreflector and the observing optics, and x is the distance between the film and the observing optics.

For human eye observation, alternative metrics need to be considered when using Eq. (6). In high ambient light (daytime) conditions, the human eye is in its highest acuity photopic response. This response relates to the use of the color recepting cones only, which are physically located in the fovea of the eye. The fovea's focusing field of view (sharp central vision) is ~2 deg,[26] which leads to a subtended background area at the location of the retroreflecting film that determines the reflected ambient saturation levels that need to be overcome to identify the retroreflection with the naked eye. This leads to the following equation for the incident background illumination (P_{AI}) from Eq. (6) being reflected back to the viewing optics (eye).

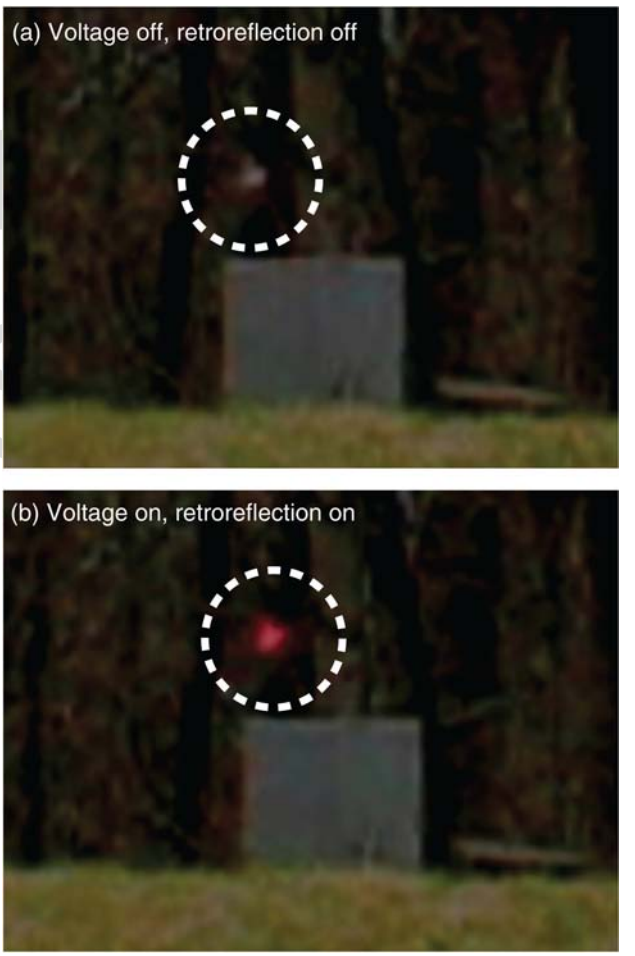

Fig. 15 Example demonstration of a switchable retroreflector (~10 × 7.5 cm) interrogated at a distance of 400 m with a 10 mW output 635 nm laser and a spot size of ~50. (a) Shows the retroreflector being illuminated (continuous wave), with no interrogated code transmission. (b) Shows the retroreflector being interrogated with the matching code, allowing retroreflection. Images were taken through a Vortex Viper HD 80 mm spotting scope with a Canon Power Shot S3 IS camera. The dashed white circle indicates where the switchable retroreflector is located. The original images have been modified.

$$P_{\mathrm{AI}} = E_V A_{\mathrm{FOV}} = E_V \pi x^2 \tan^2 \theta_{\mathrm{FOV}}, \quad (7)$$

where E_V is the ambient illuminance (lux), A_{FOV} is the area subtended by the foveal field of view, and θ_{FOV} is the foveal field of view angle. This assumes that the focal area of the eye is circular in shape.

The final threshold flux, $\varphi_{V\text{-Thres}}$ (lumens), that the eye needs to see over the ambient conditions can be expressed as

$$\phi_{V-\mathrm{Thres}} = P_{\mathrm{DA}} e^{-2\alpha x(\mathrm{km})} \eta_D R C, \quad (8)$$

which takes into consideration the ambient attenuation (α), the observation optics and detector efficiency coefficient (η_D), the reflection coefficient (R) of the surrounding surface, and the contrast change (C) needed for a given wavelength for the eye to perceive a difference in an object compared to its surroundings. The threshold flux can then be converted to its radiometric unit for the specific wavelength used for interrogation (watts). Example plots of this can be seen in Fig. 14 showing the threshold irradiances needed for visualization in various visible lighting conditions and wavelengths. Lighting conditions ranging from direct sunlight (30k lux) to overcast sunset (22 lux) are plotted. All other variables used can be seen in Table 2.

NVIS plots are also shown in Fig. 14. These were derived using the equivalent background illuminance (EBI) specification for standard GEN 3 NVIS systems. The EBI ($2.5\mathrm{E}^{-11}$ lm/cm^2) was converted to radiometric terms and then multiplied by the sensitivity at 850 nm (0.9962). The NVIS plots shown would be for using an 850-nm light source at the labeled optical powers.

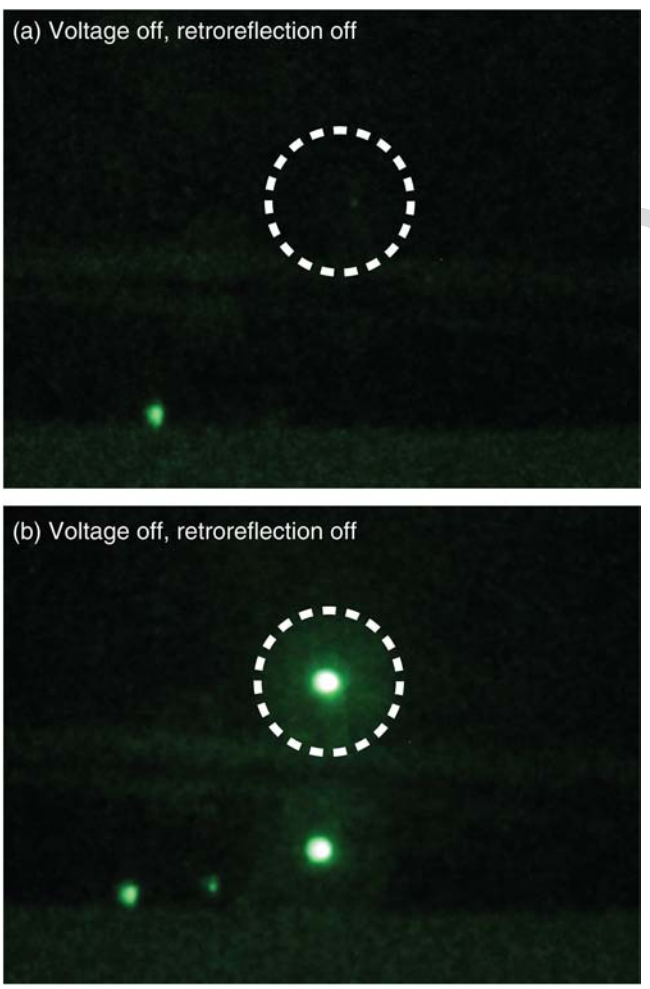

Fig. 16 Example demonstration of a switchable retroreflector (~10 × 7.5 cm) interrogated at a distance of 100 m with a 1.5 mW output 850 nm light source with an elliptical divergence of ~5.5 deg and ~4.5 deg being viewed with NVIS through a spotting scope. (a) Shows the retroreflector being illuminated (continuous wave), with no interrogated code transmission. (b) Shows the retroreflector being interrogated with the matching code, allowing retroreflection. The dashed white circle indicates where the switchable retroreflector is located. The spot that shows up below the highlighted area in (b) is the reflection off the surface of the retroreflector being reflected off the surface of a pond. The smaller spots to the left are reflections from external lights.

4 Demonstration

Demonstrations were performed in a location consisting of grassy fields and wooded deciduous backgrounds. Daytime conditions were clear (no fog/airborne particulate) of a mostly cloudy/nearly overcast sky with illuminance levels at ~18k lux as measured with a Circuit Specialists MS8209 multimeter. Interrogated distances ranged from ~50 to 400 m, the latter of which is shown in Fig. 15 using a 10 mW output 635-nm light source. Viewing and imaging were performed through a Vortex Viper HD 80 mm spotting scope. The switchable retroreflector showed sufficient contrasts for visual conspicuity. Successful electronic interrogation response was performed from ~50 to 200 m using a 2.5 mW output light source with spot sizes up to ~80 cm diameter, compared to lab condition (~5 m distance) spot sizes of ~86 cm.

Nighttime demonstrations were performed in the same location over the same distance range. An NVIS monocular device was used for viewing and imaging purposes. The light source used was a 1.5 mW output laser with peak wavelength at 850 nm. Electronic response was achieved with a spot size of ~104 cm (diameter). In comparison, lab condition measurements provided an equivalent spot size of ~147 cm. Optical response (manual switching) was achieved over the full range with the highest divergence setting (elliptical shape ~4 to 5.5 deg). This can be seen in Fig. 16.

5 Discussion and Conclusions

The system discussed and demonstrated herein provides proof-of-concept results for an optical discrimination system with PDLC based switchable retroreflective films. The switchable retroreflective film's high optical efficiency, contrast, and broad spectrum operation make it an ideal solution for enhanced conspicuity for signage, range finding, and tagging, among other possible applications. We have also shown that the switchable retroreflective films can operate over a temperature range of −15 to +95°C, fully submerged underwater, and with several induced through hole film piercing/tears lending them to be useful even in harsh environments.

The discussed setup was for proof-of-concept demonstrations with ease of alignment, interrogation, and observation in mind, and may not necessarily be useful to all industries. However, the simplicity of the system allows it to be easily integrated with existing systems by replacing static retroreflective or light-emitting tags with the switchable receiver/films we report here, and by retro-fitting light sources (light-emitting diodes/lasers) with simple encoding circuits.

The size, weight, and power consumption can be substantially reduced with further optimization and the use of application-specific integrated circuits, allowing further ease of mobility and decrease in battery change frequency.

Acknowledgments

The authors would like to thank S. Scott of Orafol Americas Inc. for providing corner-cube retrorefelective films, NGC Xetron (Cincinnati, Ohio) for their collaboration, and Dr. J. Mando, M.D., of the University of Kentucky Medical Center, for ophthalmological insight.

References

1. E. Laskowski, "Range finder wherein distance between target and source is determined by measuring scan time across a retroreflective target," U.S. Patent No. 4, 788, 441 (1988).
2. G. A. Van Lear, Jr., "Reflectors used in highway signs and warning signals, parts I, II, III," *J. Opt. Soc. Am.* **30**(10), 462–487 (1940).
3. S. J. Gerathewohl, "Conspicuity of steady and flashing light signals: variation of contrast," *J. Opt. Soc. Am.* **43**(7), 567–571 (1953).
4. D. Gunawan, L. Lin, and K. Pister, "Micromachined corner cube reflectors as a communication link," *Sens. Actuators A Phys.* **47**(1–3), 580–583 (1995).
5. W. Rabinovich and S. Bowman, "Intrinsic multiple quantum well spatial light modulators," *Appl. Phys. Lett.* **66**, 1044–1046 (1995).
6. W. Rabinovich and R. Mahon, "A cat's eye multiple quantum-well modulating retro-reflector," *Photonics* **15**(3), 461–463 (2003).
7. W. S. Rabinovich, "Free-space optical communications link at 1550 nm using multiple-quantum-well modulating retroreflectors in a marine environment," *Opt. Eng.* **44**(5), 056001 (2005).
8. W. S. Rabinovich et al., "45-Mbit/s cat's-eye modulating retroreflectors," *Opt. Eng.* **46**(10), 104001 (2007).
9. M. Pollack, R. Fair, and A. Shenderov, "Electrowetting-based actuation of liquid droplets for microfluidic applications," *Appl. Phys. Lett.* **77**(11), 1725–1726 (2000).
10. F. Mugele and J.-C. Baret, "Electrowetting: from basics to applications," *J. Phys. Condens. Matter* **17**(28), R705–R774 (2005).
11. M. K. Kilaru, B. Cumby, and J. Heikenfeld, "Electrowetting retroreflectors: scalable and wide-spectrum modulation between corner cube and scattering reflection," *Appl. Phys. Lett.* **94**(4), 041108 (2009).
12. M. K. Kilaru, J. Yang, and J. Heikenfeld, "Advanced characterization of electrowetting retroreflectors," *Opt. Express* **17**(20), 17563–17569 (2009).
13. P. Schultz, B. Cumby, and J. Heikenfeld, "Investigation of five types of switchable retroreflector films for enhanced visible and infrared conspicuity applications," *Appl. Opt.* **51**(17), 3744–3754 (2012).
14. H. D. Eckhardt, "Simple model of corner reflector phenomena," *Appl. Opt.* **10**(7), 1559–1566 (1971).
15. ORAFOL Europe GmbH, "Retroreflective Materials," 2016, http://www.orafol.com/rs/americas/en/technology (17 March 2016).
16. A. Marchant, "Conspicuity tape for enhanced laser range finding," *Opt. Eng.* **49**(4), 046401 (2010).
17. J. West, "Phase separation of liquid crystals in polymers," *J. Mol. Cryst. Liq. Cryst.* **157**(1), 427–441 (1988).
18. J. W. Mccargar, R. Ondris-crawford, and J. L. West, "Polymer dispersed liquid crystal infrared light shutter," *J. Electron. Imaging* **1**(1), 22–28 (1992).
19. J. L. West, "Characterization of polymer dispersed liquid-crystal shutters by ultraviolet/visible and infrared absorption spectroscopy," *J. Appl. Phys.* **70**(7), 3785–3790 (1991).
20. P. S. Drzaic, "Polymer dispersed nematic liquid crystal for large area displays and light valves," *J. Appl. Phys.* **60**(6), 2142–2148 (1986).
21. J. W. Doane et al., "Polymer dispersed liquid crystals for display application," *J. Mol. Cryst. Liq. Cryst.* **165**(1), 511–532 (1988).
22. G. Spruce and R. D. Pringle, "Polymer dispersed liquid crystal (PDLC) films," *Electron. Commun. Eng. J.* **4**(2), 91–100 (1992).
23. L. Mandelstam, "Light scattering by inhomogeneous media," *Zh. Russ. Fiz-Khim. Ova* **58**, 381 (1926).
24. M. Kerker, *The Scattering of Light, and Other Electromagnetic Radiation*, Academic, New York (1969).
25. J. H. Lambert, *Lamberts Photometrie:Photometria, sive De mensura et gradibus luminis, colorum et umbrae(1760)*, W Engelmann, Leipzig (1892).
26. M. D. Fairchild, *Color Appearance Models*, John Wiley & Sons, Ltd., Chichester (2013).

Phillip Schultz is the lead research and development engineer for Okeanos Technologies, LLC, working in water desalination. He received his bachelor's degree in electrical engineering in 2009, with a minor in photonics, from the University of Cincinnati. He pursued a direct to PhD route in electrical engineering, also from the University of Cincinnati, finishing his doctorate in 2013. His current research interests are water desalination, microfluidics, optics, electrowetting, electrochemistry, and devices.

Jason Heikenfeld is a professor at the University of Cincinnati. He is a senior member of IEEE and the Society for Information Display, a life member of SPIE, a member of ASEE, and a fellow of the National Academy of Inventors. In addition to scholarly work, he is an award-winning educator and has led the creation of programs and coursework that foster innovation, entrepreneurship, and understanding of the profound impact that technology has on society.